 MCB, vol.5, no.3, pp.207-216, 2008

Fung's Model of Arterial Wall Enhanced with a Failure Description

K.Y. Volokh*

Abstract: One of the seminal contributions of Y.C. Fung to biomechanics of soft tissue is the introduction of the models of arterial deformation based on the exponential stored energy functions, which are successfully used in various applications. The Fung energy functions, however, explain behavior of intact arteries and do not include a description of arterial failure. The latter is done in the present work where Fung's model is enhanced with a failure description. The description is based on the introduction of a limiter for the stored energy – the average energy of chemical bonds, which can be interpreted as a failure constant characterizing the material 'toughness'. The limiting failure energy controls materials softening, which indicates the onset of failure. We demonstrate the efficiency of the enhanced Fung formulation on a problem of the arterial inflation under internal pressure. We show, particularly, that residual stresses delay the onset of failure. The considered softening hyperelasticity approach is an alternative to the simplistic pointwise failure criteria of strength of materials on the one hand and the sophisticated approach of damage mechanics involving internal variables on the other hand.

Keyword: Artery; Failure; Anisotropy; Fung model; Softening

1 Introduction

In the 70s of the past century Y.C. Fung made pioneering contributions in the field of soft tissue mechanics and, especially, in the mechanics of the arterial wall (Fung 1990; 1993). Since then enormous progress has been made in phenomenological modeling of arteries: von Maltzahn (1981); Chuong and Fung (1983); Tözeren (1984); Demiray (1991); Wuyts et al (1995); Delfino (1997); Simon et al (1998a, 1998b), Humphrey (2002); Cowin and Humphrey (2002); Holzapfel and Ogden (2003; 2006). Some issues, nonetheless, require further elaboration. Among them is a theoretical description of arterial failure.

Two approaches to predict arterial failure are available. The first – strength of materials – approach is based on a pointwise criticality condition. According to it, material/structure failure is claimed when, for example, the maximum von Mises stress at a point reaches a critical value. Evidently, such an approach is restrictive because the local state of deformation defines global failure, which is not necessarily correct. Moreover, the critical value of the von Misses stress is defined separately from stress analysis. The drawbacks of the first approach do not exist in the second – damage mechanics – approach that allows modeling global failure and includes the failure condition in its constitutive description. In damage mechanics a scalar or tensor parameter is introduced to describe the degradation of material properties during mechanical loading. The damage parameter is an internal variable whose magnitude is constrained by a damage evolution equation and a critical threshold condition. Theoretically, the approach of damage mechanics is very flexible and allows reflecting the physical processes triggering macroscopic damage at small length scales. Practically, the experimental calibration of damage theories is far from trivial and, because of that, it is reasonable to look for alternative theories that present the bulk failure in more feasible ways than the traditional damage theories.

As a physically-based alternative to the simplistic description of strength of materials on the one hand and the sophisticated approach of damage mechanics on the other hand we present a soften-

* CEE, Technion – Israel Institute of Technology, Haifa 32000, Israel. E-mail: cvolokh@technion.ac.il. Dedicated to Y.C. Fung on his 90^{th} birth anniversary

ing hyperelasticity approach where the constitutive description of arteries is enhanced with strain softening, which is controlled by material constants. The novel approach is attractive because the new material constants can be readily calibrated in experiments and the failure description is included in the constitutive law. We use the Fung arterial model with softening for studying the effect of residual stresses on arterial failure and find that residual stresses provide delay of the failure onset.

The paper is organized as follows. The second section presents general formulae for the hyperelastic arterial wall under internal pressure. The Fung stored energy function is specified in section three where numerical solutions are generated for the experimentally calibrated materials constants. The concept of softening hyperelasticity is introduced in section four to describe the material failure. The concept is applied to the Fung model in section five where the results of numerical simulations are presented. The paper ends with a discussion in section six.

2 Artery inflation under internal pressure

We start with the classical formulation of nonlinear elasticity according to which a generic material particle of body Ω occupying position $\mathbf{X}$ at the reference state moves to position $\mathbf{x}(\mathbf{X})$ in the current configuration. The deformation of the particle is defined by the tensor of deformation gradient, $\mathbf{F} = \partial\mathbf{x}/\partial\mathbf{X}$. The boundary-value problem is set in the form

$$\mathrm{div}\,\boldsymbol{\sigma} = \mathbf{0} \quad \text{in } \Omega, \tag{1}$$

$$\boldsymbol{\sigma} = -p\mathbf{1} + \mathbf{F}\frac{\partial\psi}{\partial\mathbf{E}}\mathbf{F}^T, \tag{2}$$

$$\mathbf{x} = \overline{\mathbf{x}} \quad \text{on } \partial\Omega_{\mathbf{x}} \quad \text{or} \quad \boldsymbol{\sigma}\mathbf{n} = \overline{\mathbf{t}} \quad \text{on } \partial\Omega_{\mathbf{t}}, \tag{3}$$

where 'div' operator is with respect to the current coordinates; $\boldsymbol{\sigma}$ is the Cauchy stress tensor; $\mathbf{1}$ is the second order identity tensor; $\mathbf{E} = (\mathbf{F}^T\mathbf{F} - \mathbf{1})/2$ is the Green strain tensor; ψ is a stored energy; $\mathbf{t}$ is traction per unit area of the current surface with the unit outward normal $\mathbf{n}$; and the barred quantities are prescribed.

The Lagrange multiplier p in (2) enforces the material incompressibility assumption

$$\det\mathbf{F} = 1. \tag{4}$$

Such an assumption is often used for analysis of soft biological materials because their response to hydrostatic pressure is much stronger than their response to shearing. It seems, however, that the applicability of the incompressibility assumption essentially depends on the specific loading and deformation of the material under consideration (Volokh, 2006a).

We consider the radial inflation of an artery as a symmetric deformation of a cylinder obeying the incompressibility conditions (Fung, 1990)

$$r = \sqrt{\frac{R^2 - A^2}{\gamma s} + a^2}, \quad \theta = \gamma\Theta, \quad z = sZ, \tag{5}$$

where a point occupying position (R, Θ, Z) in the reference configuration is moving to position (r, θ, z) in the current configuration; s is the axial stretch; $\gamma = 2\pi/(2\pi - \omega)$, where ω is the artery opening angle in the reference configuration; A and a are the internal artery radii before and after deformation accordingly.

In the present work, we introduce residual stresses via the opening central angle, ω, in a stress-free reference configuration following Fung. Residual stresses are one of the most intriguing features of mechanics of living tissues (Vaishnav et al, 1973; Rachev and Greenwald, 2003). While the qualitative nature of residual stresses related with tissue growth is understood reasonably well, the best way to quantify them remains to be settled (Volokh, 2006b).

Accounting for (5), the deformation gradient and the nontrivial components of the Green strain take the following forms

$$\mathbf{F} = (R/\gamma sr)\mathbf{k}_r \otimes \mathbf{K}_R + (\gamma r/R)\,\mathbf{k}_\theta \otimes \mathbf{K}_\Theta + s\,\mathbf{k}_z \otimes \mathbf{K}_Z, \tag{6}$$

$$\begin{cases} E_{RR} = \{(R/\gamma sr)^2 - 1\}/2 \\ E_{\Theta\Theta} = \{(\gamma r/R)^2 - 1\}/2 \\ E_{ZZ} = \{s^2 - 1\}/2 \end{cases}, \tag{7}$$

where $\{\mathbf{K}_R, \mathbf{K}_\Theta, \mathbf{K}_Z\}$ and $\{\mathbf{k}_r, \mathbf{k}_\theta, \mathbf{k}_z\}$ are the orthonormal bases[1] in cylindrical coordinates at the reference and current configurations accordingly.

Accounting for (2), (6)-(8) and assuming that the stored energy depends on the nontrivial strain components only we get the following nonzero components of the Cauchy stress

$$\begin{cases} \sigma_{rr} = & -p + \frac{R^2}{(sr\gamma)^2}\frac{\partial\psi}{\partial E_{RR}} \\ \sigma_{\theta\theta} = & -p + \frac{(r\gamma)^2}{R^2}\frac{\partial\psi}{\partial E_{\Theta\Theta}} \\ \sigma_{zz} = & -p + s^2\frac{\partial\psi}{\partial E_{ZZ}} \end{cases}. \tag{8}$$

Besides, there is only one nontrivial equilibrium equation

$$\frac{\partial\sigma_{rr}}{\partial r} + \frac{\sigma_{rr} - \sigma_{\theta\theta}}{r} = 0. \tag{9}$$

The traction boundary conditions are

$$\begin{cases} \sigma_{rr}(r=a) = & -g \\ \sigma_{rr}(r=b) = & 0 \end{cases}, \tag{10}$$

where a, b are the inner and outer radii of the artery after the deformation, which were equal to A, B before the deformation accordingly; and g is the internal pressure.

We integrate equilibrium equation (9) over the wall thickness with account of boundary conditions (10) and get

$$\begin{aligned} g(a) &= -\int_a^{b(a)} (\sigma_{rr} - \sigma_{\theta\theta})\frac{dr}{r} \\ &= -\int_a^{b(a)} \left(\frac{R^2}{(\gamma sr)^2}\frac{\partial\psi}{\partial E_{RR}} - \frac{(\gamma r)^2}{R^2}\frac{\partial\psi}{\partial E_{\Theta\Theta}}\right)\frac{dr}{r}, \end{aligned} \tag{11}$$

where $b(a) = \sqrt{a^2 + (B^2 - A^2)/(\gamma s)}$.

Equation (11) presents the pressure-radius $(g-a)$ relationship, which we examine below. Before doing that, however, we introduce dimensionless variables as follows

$$\begin{aligned} &\overline{g} = \frac{g}{c}; \quad \overline{\psi} = \frac{\psi}{c}; \quad \overline{r} = \frac{r}{A}; \\ &\overline{R} = \frac{R}{A}; \quad \overline{a} = \frac{a}{A}; \quad \overline{b} = \frac{b}{A}, \end{aligned} \tag{12}$$

where the shear modulus, c, will be defined in the next section.

Substituting (12) in (11) we get

$$\overline{g}(\overline{a}) = -\int_{\overline{a}}^{\overline{b}(\overline{a})} \left(\frac{\overline{R}^2}{(\gamma s\overline{r})^2}\frac{\partial\overline{\psi}}{\partial E_{RR}} - \frac{(\gamma\overline{r})^2}{\overline{R}^2}\frac{\partial\overline{\psi}}{\partial E_{\Theta\Theta}}\right)\frac{d\overline{r}}{\overline{r}}, \tag{13}$$

where

$$\overline{b}(\overline{a}) = \sqrt{\overline{a}^2 + ((B/A)^2 - 1)/(\gamma s)}, \tag{14}$$

$$\overline{R}^2 = \gamma s(\overline{r}^2 - \overline{a}^2) + 1. \tag{15}$$

The dimensionless Lagrange multiplier $\overline{p} = p/c$ is obtained from (9) and $(10)_1$ by integration

$$\begin{aligned} \overline{p}(\overline{r}) &= \frac{\overline{R}(\overline{r})^2}{(\gamma s\overline{r})^2}\frac{\partial\overline{\psi}}{\partial E_{RR}}(\overline{r}) - \overline{g}(\overline{a}) \\ &+ \int_{\overline{a}}^{\overline{r}} \left(\frac{\overline{R}(\rho)^2}{(\gamma s\rho)^2}\frac{\partial\overline{\psi}}{\partial E_{RR}}(\rho) - \frac{(\gamma\rho)^2}{\overline{R}(\rho)^2}\frac{\partial\overline{\psi}}{\partial E_{\Theta\Theta}}(\rho)\right)\frac{d\rho}{\rho}, \end{aligned} \tag{16}$$

and normalized stresses take the form

$$\begin{cases} \overline{\sigma}_{rr} = & \frac{\sigma_{rr}}{c} = -\overline{p} + \frac{\overline{R}^2}{(s\overline{r}\gamma)^2}\frac{\partial\overline{\psi}}{\partial E_{RR}} \\ \overline{\sigma}_{\theta\theta} = & \frac{\sigma_{\theta\theta}}{c} = -\overline{p} + \frac{(\overline{r}\gamma)^2}{\overline{R}^2}\frac{\partial\overline{\psi}}{\partial E_{\Theta\Theta}} \\ \overline{\sigma}_{zz} = & \frac{\sigma_{zz}}{c} = -\overline{p} + s^2\frac{\partial\overline{\psi}}{\partial E_{ZZ}} \end{cases}. \tag{17}$$

3 Fung's arterial model

We use the exponential stored energy function to accomplish the formulation of the boundary-value problem of the previous section (Fung et al, 1979; Chuong and Fung, 1983; Fung, 1993)

$$\begin{aligned} W =& \frac{c}{2}(e^Q - 1) \\ Q =& c_1E_{RR}^2 + c_2E_{\Theta\Theta}^2 + c_3E_{ZZ}^2 + 2c_4E_{RR}E_{\Theta\Theta} \\ &+ 2c_5E_{ZZ}E_{\Theta\Theta} + 2c_6E_{RR}E_{ZZ} \end{aligned} \tag{18}$$

with c the only dimensional elastic parameter and c_i dimensionless.

We generate the pressure-radius curves (13) and stresses (19) – Figures 1 and 2 – for the following set of material parameters (Chuong and Fung,

[1] $\mathbf{K}_R = (\cos\Theta, \sin\Theta, 0)^T$; $\mathbf{K}_\Theta = (-\sin\Theta, \cos\Theta, 0)^T$; $\mathbf{K}_Z = (0,0,1)^T$; $\mathbf{k}_r = (\cos\theta, \sin\theta, 0)^T$; $\mathbf{k}_\theta = (-\sin\theta, \cos\theta, 0)^T$; $\mathbf{k}_z = (0,0,1)^T$

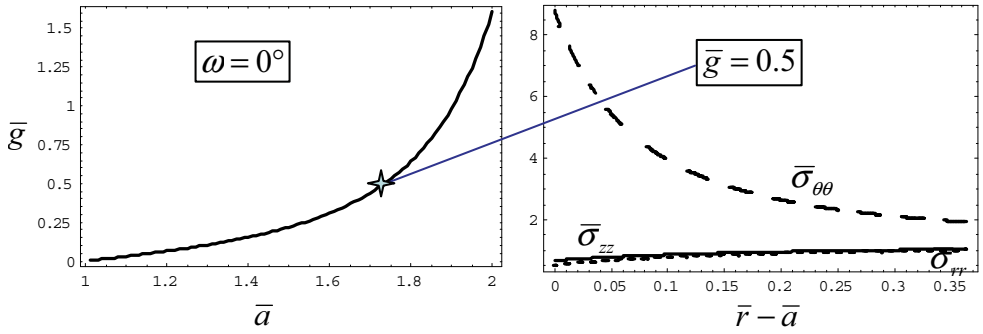

Figure 1: Pressure-radius (left) and true stresses (right) curves for artery without pre-stress.

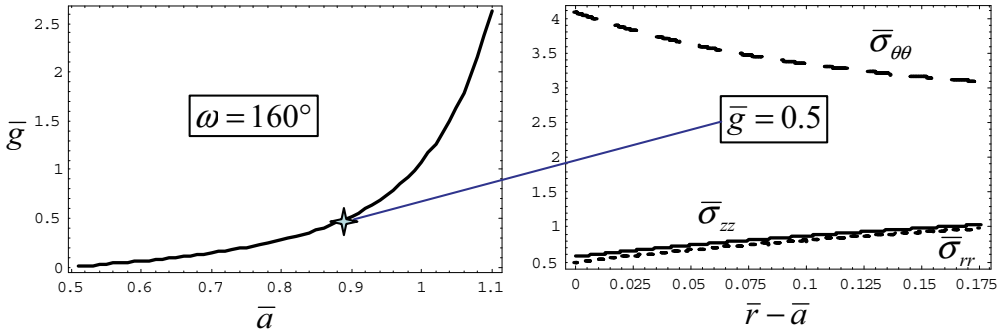

Figure 2: Pressure-radius (left) and true stresses (right) curves for artery with pre-stress.

1983; Holzapfel et al, 2000): $c_1 = 0.0089$, $c_2 = 0.9925$, $c_3 = 0.4180$, $c_4 = 0.0193$, $c_5 = 0.0749$, $c_6 = 0.0295$.

Firstly, we set an unprestressed state with $\omega = 0°$ and the internal and external reference radii $A = 0.71\,\text{mm}$ and $B = 1.10\,\text{mm}$ accordingly. The pressure-radius and stress distribution curves are calculated with the help of Mathematica (Wolfram, 2003) presented in Fig.1. We choose stress for dimensionless pressure $\overline{g} = 0.5$, which corresponds to pressure $g = 13.47\,\text{KPa}$ for the shear modulus $c = 26.95\,\text{KPa}$.

Secondly, we set a prestressed state with $\omega = 160°$ and the internal and external reference radii $A = 1.43\,\text{mm}$ and $B = 1.82\,\text{mm}$ accordingly. The pressure-radius and stress distribution curves are presented in Fig.2. We again choose stress for dimensionless pressure $\overline{g} = 0.5$, which corresponds to pressure $g = 13.47\,\text{KPa}$ for the shear modulus $c = 26.95\,\text{KPa}$.

We note that the pressure increase always corresponds to the radius increase, i.e. the artery deformation is always stable and no failure is observed. The latter is unphysical, of course, and a failure description should be included in the constitutive setting and observed on the pressure-radius curve as an onset of instability.

4 Softening hyperelasticity: microscopic motivation and macroscopic formulation

This section aims at motivating and establishing the softening hyperelasticity approach for modeling arterial failure.

Consider a solid body comprised of particles, for example molecules, placed at $\mathbf{r}_i$ in the 3D space. Generally, the volumetric density of the total potential energy of the body is a function of the particle positions: $E(\mathbf{r}_1, \mathbf{r}_2, \ldots, \mathbf{r}_N)$, where N is the number of particles. More specifically, the potential energy density, i.e. the strain energy, can be written with account of the two-particle interactions as follows

$$\psi = \frac{E}{2V} = \frac{1}{2V}\sum_{i,j} U(r_{ij}), \quad r_{ij} = \left|\mathbf{r}_{ij}\right| = \left|\mathbf{r}_i - \mathbf{r}_j\right|, \tag{19}$$

where V is the volume occupied by the system.

According to the Cauchy-Born rule (Weiner, 1983; Tadmor et al, 1996), originally applied to the crystal elasticity, the current $\mathbf{r}_{ij}$ and initial[2] (reference) $\mathbf{R}_{ij} = \mathbf{R}_i - \mathbf{R}_j$ relative positions of the same two particles can be related by the deformation gradient:

$$\mathbf{r}_{ij} = \mathbf{F}\mathbf{R}_{ij}, \tag{20}$$

where $\mathbf{F}$ is the deformation gradient – Fig.3.

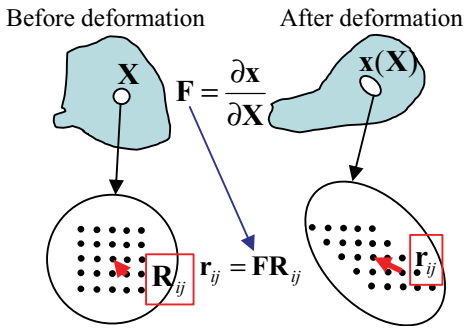

Figure 3: Cauchy-Born rule

Substituting (20) in (19) yields

$$\psi = \frac{1}{2V}\sum_{i,j} U(r_{ij}) = \psi(\mathbf{C}), \tag{21}$$

where $\mathbf{C} = \mathbf{F}^T\mathbf{F}$ is the right Cauchy-Green deformation tensor.

Direct application of (21) to analysis of material behavior can be difficult because of the large amount of particles. Gao and Klein (1998) and Klein and Gao (1998) considered the following statistical averaging procedure

$$\psi = \langle U(l)\rangle \equiv \frac{1}{V_0}\int\limits_{V_0^*} U(l) D_V dV, \tag{22}$$

$$\begin{aligned} l &= r_{ij} = L\sqrt{\boldsymbol{\xi}\cdot\mathbf{C}\boldsymbol{\xi}} = L|\mathbf{F}\boldsymbol{\xi}|, \\ L &= R_{ij} = \left|\mathbf{R}_i - \mathbf{R}_j\right|, \\ \boldsymbol{\xi} &= (\mathbf{R}_i - \mathbf{R}_j)/L, \end{aligned} \tag{23}$$

[2] We note that finding the initial equilibrium bond length can generally require a numerical minimization procedure. Moreover, the interatomic forces may differ from zero for pairs of atoms though the average force can be assumed zero.

where V_0 is the reference representative volume; l is the current virtual bond length; $U(l)$ is the bonding potential; D_V is the volumetric bond density function; and V_0^* is the integration volume defined by the range of influence of U.

Let us choose the Lennard-Jones potential to be specific in further considerations

$$V(l) = 4\varepsilon((\sigma/l)^{12} - (\sigma/l)^6), \tag{24}$$

where ε and σ are the *bond energy* and length constants – Fig.4. The minimum of $V = -\varepsilon$ is reached at the equilibrium bond length $l = \sqrt[6]{2}\sigma$ where no forces are acting between the atoms.

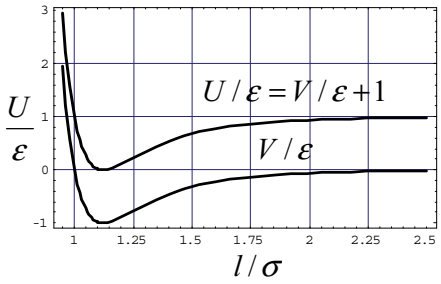

Figure 4: Lennard-Jones potential

In view of the continuum-atomistic link discussed above, we shift the energy expression (24) by ε to provide the zero minimum energy of the referential equilibrium state of the bond deformation

$$U(l) = 4\varepsilon((\sigma/l)^{12} - (\sigma/l)^6) + \varepsilon. \tag{25}$$

Then (22) takes form

$$\begin{aligned} \psi(\mathbf{C}) = \frac{1}{V_0}\int\limits_{V_0^*} \Big(4\Big(\sigma/L\sqrt{\boldsymbol{\xi}\cdot\mathbf{C}\boldsymbol{\xi}}\Big)^{12} \\ -4\Big(\sigma/L\sqrt{\boldsymbol{\xi}\cdot\mathbf{C}\boldsymbol{\xi}}\Big)^{6} + 1\Big)\varepsilon D_V dV. \end{aligned} \tag{26}$$

We can define *the average bond energy* by setting the unlimited increase of deformation

$$\Phi = \psi(\|\mathbf{C}\| \to \infty) = \frac{1}{V_0}\int\limits_{V_0^*} \varepsilon D_V dV, \tag{27}$$

where $\|\mathbf{C}\| = \sqrt{\boldsymbol{\xi}\cdot\mathbf{C}\boldsymbol{\xi}}$ for any $\boldsymbol{\xi}$.

Thus, *the average bond energy sets a limit for the energy accumulation in deformation*. This conclusion generally does not depend on the choice of the atomic potential and it is valid for any interaction that includes a possible atomic separation – the bond energy.

Contrary to the above conclusion traditional hyperelastic models of materials do not include the energy limiter. The stored energy of hyperelastic materials is defined as

$$\psi = W. \tag{28}$$

Here W is used for the strain energy of the *intact* material, which can be characterized as follows

$$\|\mathbf{C}\| \to \infty \Rightarrow \psi = W \to \infty, \tag{29}$$

where $\|\ldots\|$ is a tensorial norm.

In other words, the increasing strain increases the accumulated energy unlimitedly. Evidently, the consideration of only intact materials is restrictive and unphysical. The energy increase of a real material should be limited as it was shown above,

$$\|\mathbf{C}\| \to \infty \Rightarrow \psi = \Phi = \text{constant}, \tag{30}$$

where the average bond energy, $\Phi = \text{constant}$, can be called the *material failure energy*.

Equation (30) presents the fundamental idea of introducing a limiter of the stored energy in the elasticity theory. Such a limiter induces material softening, indicating material failure, automatically. The choice of the limited stored energy expression should generally be material-specific. Nonetheless, a somewhat universal formula (Volokh, 2007) can be introduced to enrich the already existing models of intact materials with the failure description

$$\psi(W) = \Phi - \Phi \exp(-W/\Phi). \tag{31}$$

where $\psi(W=0) = 0$ and $\psi(W=\infty) = \Phi$.

Formula (31) obeys condition $\|\mathbf{C}\| \to \infty \Rightarrow \psi(W(\mathbf{C})) = \Phi$ and, in the case of the intact material behavior, $W \ll \Phi$, we have $\psi(W) \approx W$ preserving the features of the intact material.

The constitutive equation can be written in the general form accounting for (31)

$$\begin{aligned} \boldsymbol{\sigma} &= 2J^{-1}\mathbf{F}\frac{\partial \psi}{\partial \mathbf{C}}\mathbf{F}^T \\ &= 2J^{-1}\mathbf{F}\frac{\partial W}{\partial \mathbf{C}}\mathbf{F}^T \exp(-W/\Phi), \end{aligned} \tag{32}$$

where $\boldsymbol{\sigma}$ is the Cauchy stress tensor; $J = \det \mathbf{F}$; and the exponential multiplier enforces material softening. Constitutive equation (32) is especially effective for incompressible soft materials undergoing finite deformations.

We emphasize finally that the best form of the energy function can be material/problem-specific. It is important, however, that a possible form of the energy function should limit the energy increase.

5 Fung's arterial model with the failure description

Following previous section we enhance Fung's model with softening

$$\begin{aligned} \psi =& \Phi - \Phi \exp(-c(e^Q - 1)/2\Phi) \\ Q =& c_1 E_{RR}^2 + c_2 E_{\Theta\Theta}^2 + c_3 E_{ZZ}^2 + 2c_4 E_{RR} E_{\Theta\Theta} \\ &+ 2c_5 E_{ZZ} E_{\Theta\Theta} + 2c_6 E_{RR} E_{ZZ} \end{aligned} \tag{33}$$

We again generate the pressure-radius curves (13) and stresses (19) for the same set of material parameters: $c_1 = 0.0089$, $c_2 = 0.9925$, $c_3 = 0.4180$, $c_4 = 0.0193$, $c_5 = 0.0749$, $c_6 = 0.0295$. We repeat analyses shown in Figs.1 and 2 for $\overline{\Phi} = \Phi/c = 1; 2; 3$. The results are shown in Figs. 5-10 accordingly.

We note first of all that failure appears on the pressure radius curve as a limit point where static instability occurs. Though the decreasing branch of the curve is shown for the sake of consistency, it should be clearly realized that it is not statically stable and the dynamic failure propagation should be monitored after the limit point.

There are two important features of behavior of the arterial failure presented in Figs. 5-10. Firstly, residual stresses delay the onset of failure. Interestingly the delay increases with the increasing average bond energy, Φ. Let us define pre-stress factor $\varsigma = \left|\overline{g}_c^p - \overline{g}_c\right| / \left|\overline{g}_c\right| \cdot 100\%$, where $\overline{g}_c^p$ is the critical pressure for a prestressed artery while $\overline{g}_c$

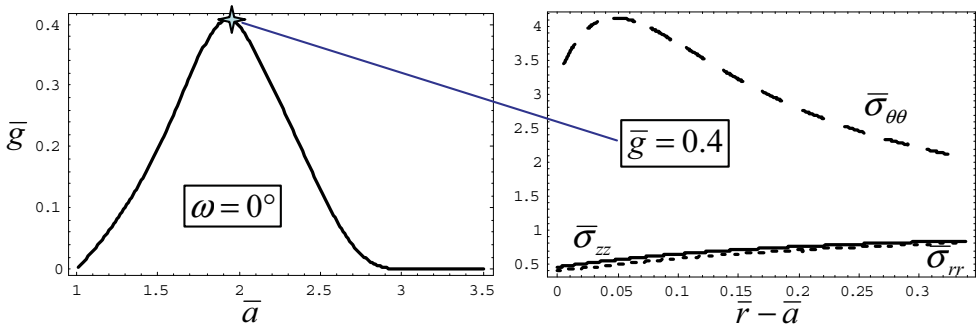

Figure 5: Pressure-radius (left) and true stresses (right) curves for $\overline{\Phi} = \Phi/c = 1$ without pre-stress.

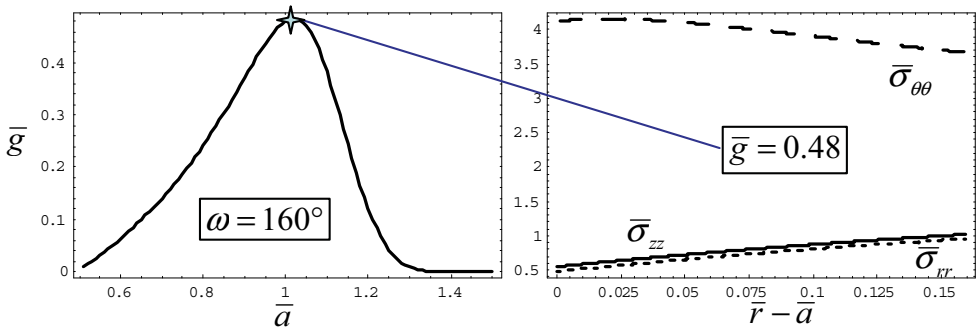

Figure 6: Pressure-radius (left) and true stresses (right) curves for $\overline{\Phi} = \Phi/c = 1$ with pre-stress.

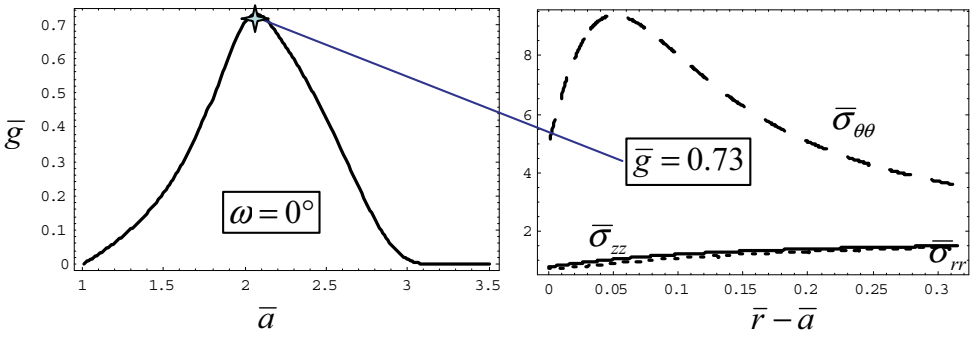

Figure 7: Pressure-radius (left) and true stresses (right) curves for $\overline{\Phi} = \Phi/c = 2$ without pre-stress.

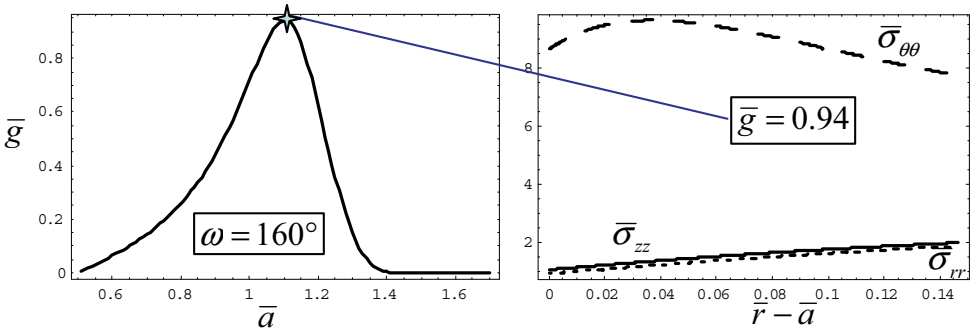

Figure 8: Pressure-radius (left) and true stresses (right) curves for $\overline{\Phi} = \Phi/c = 2$ with pre-stress.

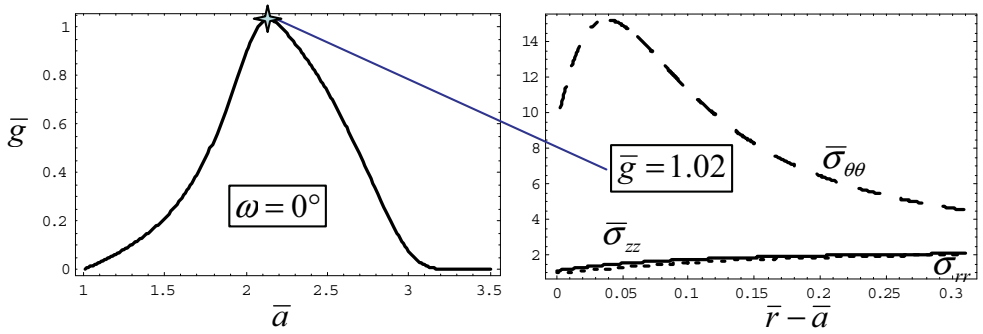

Figure 9: Pressure-radius (left) and true stresses (right) curves for $\overline{\Phi} = \Phi/c = 3$ without pre-stress.

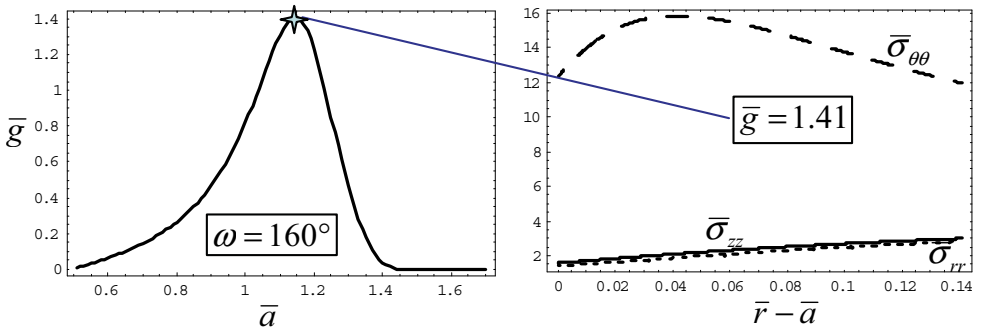

Figure 10: Pressure-radius (left) and true stresses (right) curves for $\overline{\Phi} = \Phi/c = 3$ with pre-stress.

is the critical pressure for an unprestressed artery, then the factor changes as shown in Table 1.

Table 1

$\overline{\Phi}$	1	2	3
$\varsigma(\%)$	20	29	38

Secondly, the prestress makes the distribution of the hoop stresses more uniform. In a sense, the prestress optimizes the stress distribution in a loaded artery.

6 Discussion and conclusions

A novel softening hyperelasticity model of the arterial wall was presented to allow for a description of arterial failure. This model enhances the Fung arterial model with a failure description. The latter is achieved by the introduction of the energy limiter – the average bond energy, which controls material softening. The softening is embedded in the constitutive description and it indicates the failure onset. Introduction of the new model was motivated by the necessity to give a more comprehensive failure description than the local critical stress criterion of strength of materials on the one hand and to give a simpler approach to the failure description than damage mechanics on the other hand.

Failure analysis based on the softening hyperelasticity approach allows tracking a global load-displacement path of an artery as shown in Figs. 5-10. The critical (limit) point corresponds to the onset of instability of the static deformation path. The instability occurs when the material, media or adventitia, fails locally, i.e. the molecular bonds tear, and the local failure develops. The post-critical evolution corresponding to the decreasing branches on the load-displacement curve requires, generally, a dynamic consideration. The use of the softening hyperelasticity for the dynamic failure propagation, however, is beyond the scope of the present work.

The proposed model was applied to the problem of the artery inflation under internal pressure. Numerical simulations led to the following two find-

ings. Firstly, it was found that residual stresses can increase the overall arterial strength significantly. The pre-existing compression in arteries delays the onset of rupture like the pre-existing compression in the pre-stressed concrete delays the crack opening. More experiments are welcome to clarify this interesting issue. Secondly, it was found that the prestress makes the distribution of the hoop stresses more uniform. In a sense, the prestress optimizes the stress distribution in a loaded artery.

References

1.Chuong, C.J.; Fung, Y.C. (1983): Three-dimensional stress distribution in arteries. *Journal of Biomechanical Engineering* 105, 268-274.

2.Cowin, S.C.; Humphrey, J.D. (2002): *Cardiovascular Soft Tissue Mechanics*. Springer, New York.

3.Delfino, A.; Stergiopulos, N.; Moore, J.E.; Meister, J.-J. (1997): Residual strain effects on the stress field in a thick wall finite element model of the human carotid bifurcation. *Journal of Biomechanics* 30, 777–786.

4.Demiray, H. (1991): A layered cylindrical shell model for an aorta. *International Journal of Engineering Sciences* 29, 47–54.

5.Fung, Y.C. (1990): *Biomechanics: Motion, Flow, Stress, and Growth*. Springer-Verlag, New York.

6.Fung, Y.C. (1993): *Biomechanics: Mechanical Properties of Living Tissues*. 2^{nd} ed., Springer-Verlag, New York.

7.Fung, Y.C.; Fronek, K.; Patitucci, P., (1979): Pseudoelasticity of arteries and the choice of its mathematical expression. *American Journal of Physiology* 237, H620–H631.

8.Gao, H.; Klein, P. (1998): Numerical simulation of crack growth in an isotropic solid with randomized internal cohesive bonds. *Journal of the Mechanics and Physics of Solids* 46, 187-218.

9.Holzapfel, G.A.; Gasser, T.C.; Ogden, R.W. (2000): A new constitutive framework for arterial wall mechanics and a comparative study of material models. *Journal of Elasticity* 61, 1-48.

10.Holzapfel, G.A.; Ogden, R.W. (2003): *Biomechanics of Soft Tissues in Cardiovascular Systems*. Springer, Wien.

11.Holzapfel, G.A.; Ogden, R.W. (2006): *Mechanics of Biological Tissue*. Springer, Wien.

12.Humphrey, J.D. (2002): *Cardiovascular Solid Mechanics: Cells, Tissues, and Organs*. Springer, New York.

13.Klein, P.; Gao, H. (1998): Crack nucleation and growth as strain localization in a virtual-bond continuum. *Engineering Fracture Mechanics* 61, 21-48.

14.von Maltzahn, W.-W.; Besdo, D.; Wiemer, W. (1981): Elastic properties of arteries: A nonlinear two-layer cylindrical model. *Journal of Biomechanics* 14, 389–397.

15.Rachev, A.; Greenwald, S.E., (2003): Residual stresses in conduit arteries. *Journal of Biomechanics* 36, 661-670.

16.Simon, B.R.; Kaufmann, M.V.; McAfee, M.A.; Baldwin, A.L. (1998a): Porohyperelastic finite element analysis of large arteries using ABAQUS. *Journal of Biomechanical Engineering* 120, 296–298.

17.Simon, B.R.; Kaufmann, M.V.; McAfee, M.A.; Baldwin, A.L.; Wilson, L.M. (1998b): Identification and determination of material properties for porohyperelastic analysis of large arteries. *Journal of Biomechanical Engineering* 120, 188-194.

18.Tadmor, E.B.; Ortiz, M.; Phillips, R. (1996): Quasicontinuum analysis of defects in solids. *Philosophical Magazine* 73, 1529-1563.

19.Tözeren, A. (1984): Elastic properties of arteries and their influence on the cardiovascular system. *Journal of Biomechanical Engineering* 106, 182-185.

20. Vaishnav, R.N.; Young, J.T.; Patel, D.J. (1973): Distribution of stresses and of strain-energy density through the wall thickness in a canine aortic segment. *Circulation Research*, 32, 577-583.

21. Volokh, K.Y. (2006a): Compressibility of arterial wall in ring-cutting experiments. *Molecular and Cellular Biomechanics* 3, 35-42.

22. Volokh, K.Y. (2006b): Stresses in growing soft tissues. *Acta Biomaterialia* 2, 493-504.

23. Volokh, K.Y. (2007): Hyperelasticity with softening for modeling materials failure. *Journal of the Mechanics and Physic of Solids* 55, 2237-2264.

24. Weiner, J.H. (1983): *Statistical mechanics of elasticity*. Wiley, New York.

25. Wolfram, S. (2003): *The Mathematica Book*. 5^{th} edn. Wolfram Media.

26. Wuyts, F.L.; Vanhuyse, V.J.; Langewouters, G.J.; Decraemer, W.F.; Raman, E.R.; Buyle, S. (1995): Elastic properties of human aortas in relation to age and atherosclerosis: A structural model. *Physics in Medicine and Biology* 40, 1577-1597.